ELSEVIER

NeuroImage

www.elsevier.com/locate/ynimg
NeuroImage 36 (2007) 645–660

Characterizing brain anatomical connections using diffusion weighted MRI and graph theory

Y. Iturria-Medina,[a,*] E.J. Canales-Rodríguez,[a] L. Melie-García,[a] P.A. Valdés-Hernández,[a] E. Martínez-Montes,[b] Y. Alemán-Gómez,[a] and J.M. Sánchez-Bornot[b]

[a]*Neuroimaging Department, Cuban Neuroscience Center, Avenue 25, Esq 158, #15202, PO Box 6412, Cubanacán, Playa, Havana, Cuba*
[b]*Neurostatistic Department, Cuban Neuroscience Center, Havana, Cuba*

Received 24 July 2006; revised 1 February 2007; accepted 6 February 2007
Available online 15 February 2007

A new methodology based on Diffusion Weighted Magnetic Resonance Imaging (DW-MRI) and Graph Theory is presented for characterizing the anatomical connections between brain gray matter areas. In a first step, brain voxels are modeled as nodes of a non-directed graph in which the weight of an arc linking two neighbor nodes is assumed to be proportional to the probability of being connected by nervous fibers. This probability is estimated by means of probabilistic tissue segmentation and intravoxel white matter orientational distribution function, obtained from anatomical MRI and DW-MRI, respectively. A new tractography algorithm for finding white matter routes is also introduced. This algorithm solves the most probable path problem between any two nodes, leading to the assessment of probabilistic brain anatomical connection maps. In a second step, for assessing anatomical connectivity between K gray matter structures, the previous graph is redefined as a K+1 partite graph by partitioning the initial nodes set in K non-overlapped gray matter subsets and one subset clustering the remaining nodes. Three different measures are proposed for quantifying anatomical connections between any pair of gray matter subsets: Anatomical Connection Strength (ACS), Anatomical Connection Density (ACD) and Anatomical Connection Probability (ACP). This methodology was applied to both artificial and actual human data. Results show that nervous fiber pathways between some regions of interest were reconstructed correctly. Additionally, mean connectivity maps of ACS, ACD and ACP between 71 gray matter structures for five healthy subjects are presented.
© 2007 Elsevier Inc. All rights reserved.

Keywords: Brain connectivity; Diffusion weighted magnetic resonance imaging; Graph model; Tractography

Introduction

Random motion of water molecules inside the brain is influenced by the architectural properties of tissues. Water diffusion is known to be highly anisotropic in certain white matter regions, with preferential movement along the nervous fibers. A recent development of a non-invasive technique which quantifies water diffusion process, known as Diffusion Weighted Magnetic Resonance Imaging (DW-MRI), has allowed to obtain structural information about the intravoxel axon arrangement (Basser et al., 1994; LeBihan, 2003). Based on this information, fiber tractography arises as a crucial technique to attain a better in vivo anatomical characterization of the brain (Mori et al., 1999; Conturo et al., 1999; Tuch, 2002; Parker et al., 2002; Koch et al., 2002; Behrens et al., 2003). Also, quantification of the anatomical connectivity between different gray matter structures would be a significant contribution to the understanding of functional integration of the human brain (LeBihan et al., 2001; Koch et al., 2002; Ramnani et al., 2004; Sporns et al., 2005; Sotero et al., 2007).

Reconstruction of nervous fiber trajectories is an extensively treated topic. In the traditional Streamline Tractography (SLT) approach (Mori et al., 1999; Conturo et al., 1999; Basser et al., 2000), a continuous trajectory is traced tangential to the direction of the principal eigenvector of the diffusion tensor measured at each voxel using a discretization step smaller than the size of the voxel. This approach usually fails in voxels where fibers cross each other, merge, kiss or diverge, and it is very sensitive to the influence of MR signal noise (Basser and Pajevic, 2000; Lori et al., 2002). In those situations, traced path strays from the real trajectory of nervous fibers. To overcome these limitations, modified Streamline Tractography (mSLT) methods based on Diffusion Tensor Deflection (Weinstein et al., 1999; Lazar et al., 2003) and Probabilistic Monte-Carlo Method (Parker and Alexander, 2003) have been proposed. The former uses the entire diffusion tensor to deflect the propagation direction computed in the previous step. The latter uses the uncertainty of the estimated nervous fiber orientation to compute a large number of possible paths from the seed point; a quantity can be assigned to each path reflecting some connectivity relationship between seed and target points.

In recent years, many other mSLT methods have been proposed (Tuch, 2002; Tench et al., 2002; Behrens et al., 2003; Hagmann et al., 2003). Usually, they define the anatomical connection pro-

* Corresponding author. Fax: +53 7 208 6707.
E-mail address: iturria@cneuro.edu.cu (Y. Iturria-Medina).
Available online on ScienceDirect (www.sciencedirect.com).

1053-8119/$ - see front matter © 2007 Elsevier Inc. All rights reserved.
doi:10.1016/j.neuroimage.2007.02.012

bability between seed and target voxels as the ratio between the number of shared paths and the number of generated paths.

In contrast to SLT and mSLT methods, Level Set-Based Fast Marching (FM) techniques (Parker et al., 2002; Staempfli et al., 2006) express the tractography in terms of a wave front that emanates from a source point and whose evolution is controlled by the diffusion data. FM methods have two advantages over the SLT and mSLT methods: 1, better performance in situations of branching and fiber crossing, and 2, direct estimation of the probability of white matter connectivity between two points (Jun Zhang et al., 2005).

In FM methods, front evolution speed and direction in a voxel depend on the measured diffusion tensor. Generally, all proposed FM algorithms have used only the principal eigenvector of the diffusion tensor, therefore these methods fail to reconstruct fiber pathways in those places where fibers cross, merge, kiss or diverge. For dealing with this limitation, recently Staempfli et al. (2006) proposed an advanced implementation of FM (aFM), combining the advantages of classical FM and the tensor deflection approach. The objective is to take into account the entire information contained in the diffusion tensor. As an intrinsic limitation, aFM needs an empirical threshold value to classify geometrically the diffusion tensor ellipsoid (i.e. prolate, oblate or spherical tensor) and therefore to set the corresponding speed function. Also, only four possible situations of voxel transitions are considered, which are those involving prolate and oblate cases. Thus, some combinations of more than two fibers crossing may be ignored.

On the other hand, although probability of connection between seed and target voxels has been previously used (Tuch, 2002; Parker et al., 2002; Koch et al., 2002; Parker et al., 2003; Behrens et al., 2003; Staempfli et al., 2006), the generalization of this concept to characterize anatomical connections between different brain gray matter structures is not straightforward. An initial approach (Iturria-Medina et al., 2005) was proposed to quantify the anatomical connection strength (ACS) between two gray matter structures using geometrical information from probabilistic fiber paths. ACS was considered proportional to the total area comprised by the fiber connector volume over the surfaces of the two connected structures. This was evaluated by counting the number of superficial voxels involved in the connection, where each voxel is weighted according to the validity of the paths that connect it with the second structure. A connectivity matrix estimated using the aforementioned approach was employed to couple several brain areas in a realistic neural mass model for the EEG generation, obtaining physiologically plausible results (Sotero et al., 2007).

In addition, recently Hagmann et al. (2006) proposed a technique based on graph theory to study the connectivity between small cortical areas. Nodes of a graph correspond to small cubic regions of interest (ROI) covering the brain gray matter. Fiber tractography is performed by initiating fibers over the whole brain and arc weight between any two ROIs is assigned according to the connection density between them. An unweighted version of this graph was constructed in order to analyze its small world and hierarchical properties.

In this work, our interest lies in the development of a DW-MRI-based methodology, capable of characterizing directly anatomical connections between brain gray matter structures, which can be defined according to cytoarchitectonic, histological or other sort of anatomical and functional information. In order to accomplish this, the graph framework is employed to introduce a new anatomical connectivity model. Firstly, each voxel of the cerebral volume is assumed to be a node of a non-directed weighted graph. In this case, the weight of an arc is considered to be proportional to the probability of the existence of a nervous fiber connecting its corresponding nodes. Probabilistic tissue segmentation and intravoxel white matter orientational distribution function (ODF) are combined to compute the arc weight. Secondly, an iterative algorithm is used to solve the most probable path problem between any two nodes in the graph, which we will indistinctly refer to as the most reliable connection route between these nodes. This approach allows to asses probabilistic anatomical connectivity maps between brain voxels. Finally, in order to assessing anatomical connectivity between K gray matter structures, the graph is partitioned in the corresponding K non-overlapped subsets and one subset containing the remaining nodes. This allowed for the definition of three different anatomical connectivity measures between any pair of gray matter structures: Anatomical Connection Strength (ACS), Anatomical Connection Density (ACD) and Anatomical Connection Probability (ACP).

Methods

This section will be devoted to present some basic elements of graph theory, as well as the principal steps of the proposed methodology: 1, definition of a Brain Graph, 2, introduction of an iterative fiber tracking algorithm and quantification of node–node connectivity and 3, definition of anatomical connectivity measures between gray matter areas. Details on experimental data to be used and its preprocessing will also appear.

Elements of graph theory

A graph $G=[N,A]$ is defined by a set N of n elements called nodes and a set A of elements called arcs (Gondran and Minoux, 1984). Arcs link pairs of nodes. The number of elements of a set N is known as the cardinality of N and it is denoted by $|N|$. Given an arc $a_{i,j}$ linking r_i and r_j nodes ($i, j=1,\ldots,n$), we will refer to r_i as the initial endpoint and to r_j as the terminal endpoint of $a_{i,j}$. A non-directed graph is that in which the direction of the arcs (i.e. distinction between initial and terminal nodes) is not established. Graphically, nodes are represented by points and arcs by lines (without arrow) joining them.

A graph $G=[N,A]$ is called K partite if the set of its n nodes admits a partition into K pairwise disjoint independent subsets (see Fig. 1). A path $\rho_{i_1\ldots iL}$, with $L-1$ steps, between nodes r_{i_1} and r_{i_L} is an ordered subset of $L-1$ arcs $\{a_{i_1i_2}; a_{i_2i_3};\ldots; a_{i_{L-1}i_L}\}$.

Each arc $a\in A$ is assigned a number $w(a)\in\mathcal{R}$, denominated the weight of the arc. A very large number of path finding problems in graph theory use the weight of the arc to optimize convenient cost functions. For example, if the weight of an arc is defined as its length, the problem of the shortest path between two nodes is equivalent to find the path with the minimum sum of its arc weights. Similarly, the weight of the arc can be interpreted as the cost of transportation along it, the time required to pass through it or the probability of its existence. Specifically, in a weighted non-directed graph, where each arc weight is considered as the probability of its existence, the problem of searching the most probable path between nodes r_{i_1} and r_{i_L} is equivalent to find the path $\rho_{i_1\ldots iL}$ with maximum total probability:

$$P[\rho_{i_1\ldots i_L}] = w(a_{i_1i_2}) \prod_{k=2}^{L-1} w^{\mathrm{cond}}(a_{i_ki_{k+1}}|a_{i_{k-1}i_k}), \quad (1)$$

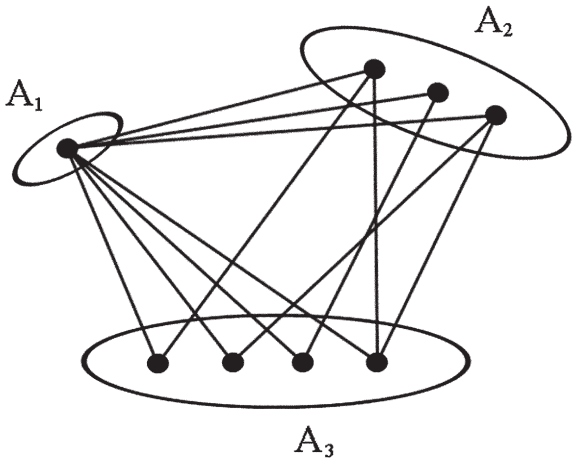

Fig. 1. Schematic representation of a multi partite graph (specifically, a tripartite graph). An initial graph of 8 nodes is partitioned in three disjoint independent node subsets, A1, A2 and A3, with 1, 3 and 4 nodes, respectively.

where the term $w^{\text{cond}}\left(a_{i_k i_{k+1}} | a_{i_{k-1} i_k}\right)$ is the conditional weight of the arc $a_{i_k i_{k+1}}$ given arc $a_{i_{k-1} i_k}$.

Defining a brain graph

Consider an orthogonal grid defining voxels $\{\vec{r}_i=(x_i,y_i,z_i); i=1..n\}$ in the space of a magnetic resonance image (or other neuroimaging technique) with anatomical information about the brain (e.g. a T1-weighted image or a Computer Tomography image). Let N be the set of voxels having a non-zero probability of belonging to some cerebral tissue. Then, we define as a Brain Graph the weighted non-directed graph $G_{\text{brain}}=[N,A]$ where A is the set of white matter links between contiguous voxels in N. Graphically, G_{brain} is a discrete set of points (nodes) representing voxels and a set of lines (arcs) representing connections between contiguous voxels (see Fig. 2a).

The weight of an arc is chosen so that it represents the probability that linked nodes are really connected by nervous fibers. A nearest neighborhood of the i-th node, denoted as N_i^{neig}, is the set of all its contiguous nodes. In our orthogonal grid, the maximum cardinality of N_i^{neig} is 26.

In the present approach, arc weight $w(a_{ij})$ $(a_{ij}\in A)$ is proposed to take into account both the probability of nodes $\vec{r}_i$ and $\vec{r}_j$ to belong to gray/white matter and the probability of nervous fibers to be oriented around the direction of the arc a_{ij}. Mathematically:

$$\begin{aligned} w(a_{ij}) &\equiv w(a_{ji}) \\ &= P_{\text{mat}}(\vec{r}_i) P_{\text{mat}}(\vec{r}_j)\left[P_{\text{diff}}(\vec{r}_i,\Delta\vec{r}_{ij}) + P_{\text{diff}}(\vec{r}_j,\Delta\vec{r}_{ji})\right], \end{aligned} \tag{2}$$

where the two basics functions P_{mat} and P_{diff} enclose anatomical and diffusion information respectively (Fig. 2b). The first of these functions is defined as follows:

$$P_{\text{mat}}(\vec{r}) = \frac{\alpha P_{\text{WM}}(\vec{r}) + P_{\text{GM}}(\vec{r})}{1+(\alpha-1)P_{\text{WM}}(\vec{r})}, \tag{3}$$

where P_{WM} and P_{GM} are probabilistic maps of white and gray matter (WM and GM) respectively and α is a tuning parameter. As we hope to associate arcs in G_{brain} to probable nervous fiber pathways, the presence of white matter (given by P_{WM}) to arc weights could be enhanced by making $\alpha \geq 1$.

The other function, $P_{\text{diff}}(\vec{r}_j,\Delta\vec{r}_{ij})$, characterizes fiber coherence along $\Delta\vec{r}_{ij}=\vec{r}_j-\vec{r}_i$, which is the direction of the arc a_{ij}, and can be inferred from DW-MRI images using methods for the description of the intravoxel white matter structure. Here, $P_{\text{diff}}(\vec{r}_j,\Delta\vec{r}_{ij})$ is assumed to be the integral of the ODF over a solid angle β around $\Delta\vec{r}_{ij}$ (Fig. 3):

$$P_{\text{diff}}(\vec{r}_i,\Delta\vec{r}_{ij}) = \frac{1}{Z}\int_{\beta} \text{ODF}(\vec{r}_i,\Delta\vec{r}_{ij})\text{d}S. \tag{4}$$

Z is a normalization constant chosen to fix to 0.5 the maximum value of the set $\left\{P_{\text{diff}}(\vec{r}_i,\Delta\vec{r}_{ij})\right\}_{\forall\vec{r}_j\in N_i^{\text{neig}}}$. Note that generally $P_{\text{diff}}(\vec{r}_i,\Delta\vec{r}_{ij}) \neq P_{\text{diff}}(\vec{r}_j,\Delta\vec{r}_{ji})$.

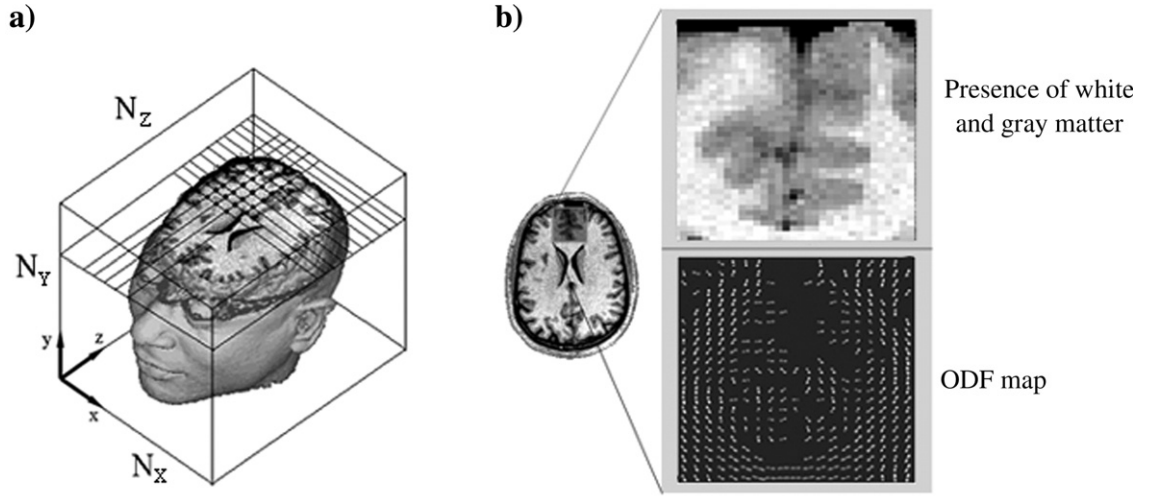

Fig. 2. Basic elements of the non-directed weighted Brain Graph G_{brain}. (a) Each voxel of the T1-weighted image volume (of dimensions N_X, N_Y, $N_Z\in\mathbb{N}$) belonging to the brain tissue is considered a node in G_{brain}. (b) Anatomical information about the presence of white and gray matter and orientational distribution function (ODF) maps are used to define the weights of the arcs in G_{brain}. Each ODF is a 3-D representation of the fiber orientation within a single voxel.

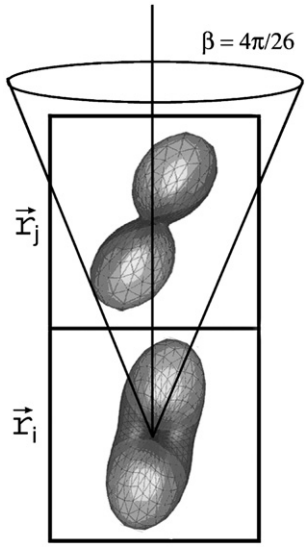

Fig. 3. The solid angle β around vector $\Delta\vec{r}_{ij}$ defines a cone in which the nervous fibers passing from node $\vec{r}_i$ to node $\vec{r}_j$ should be contained. It is defined for all 26 nearest neighbors in the same way.

Eq. (2) quantitatively combines the information of probabilistic tissue segmentation of the brain and diffusion weighted MRI data. This ensures that only those pairs of nodes with high probability of belonging to gray/white matter and high probability of sharing fibers will have higher weights, which is equivalent to have high probability of being connected. It should be kept in mind that the DW-MRI profile is symmetric under the transformation: $\vec{r} \rightarrow -\vec{r}$. This hinders the possibility to distinguish between efferent and afferent projections in a nervous tracking process.

Fiber tracking and node–node connectivity

In this work, the key idea on which fiber tracking and node-node connectivity is based derives from "the most probable path problem" between nodes of interest in the defined Brain Graph. Initially, we assumed that any possible path between these nodes corresponds to the anatomic trajectory of a probable nervous fiber. Then, an iterative algorithm is employed for finding the most probable trajectory, which is considered to evaluate the real existence of fiber pathways between these points.

Considering a given path $\rho_{s\ldots p}$, with L-1 steps, that belongs to the set of all possible paths between nodes $\vec{r}_s$ and $\vec{r}_p$; the weights of any two consecutives arcs $a_{i_{k-1}i_k}$ and $a_{i_k i_{k+1}}$ are not independent, since they share the term $P_{mat}(\vec{r}_{i_k})$. Given the existence of arc $a_{i_{k-1}i_k}$, the conditional weight of arc $a_{i_k i_{k+1}}$ results:

$$w^{cond}(a_{i_k i_{k+1}}|a_{i_{k-1}i_k}) = P_{mat}(\vec{r}_{i_{k+1}})\cdot\left[P_{diff}(\vec{r}_{i_k},\Delta\vec{r}_{i_k i_{k+1}}) + P_{diff}(\vec{r}_{i_{k+1}},\Delta\vec{r}_{i_{k+1}i_k})\right]. \quad (5)$$

In order to consider physiological and anatomical evidences about fiber bundles shape in the brain as a priori information, a modified version of Eq. (1) includes a function ψ which penalizes path curvature, as used in other tracking methods (see for example Tuch, 2002):

$$P[\rho_{s\ldots p}] = w(a_{s,i_2})\prod_{k=2}^{L\text{-}1} w^{cond}(a_{i_k i_{k+1}}|a_{i_{k-1}i_k})\Psi(\rho_{i_{k-1}\ldots i_{k+1}}), \quad (6)$$

where

$$\Psi(\rho_{i_{k-1}\ldots i_{k+1}}) = \begin{cases} f(\phi) & \text{if } \phi < \phi_{critical} \\ 0 & \text{otherwise} \end{cases}.$$

The angle ϕ is defined using the two arcs of the subpath $\rho_{i_{k-1}\ldots i_{k+1}}$:

$$\phi = \arccos\left(\frac{\Delta\vec{r}_{i_k i_{k+1}}\Delta\vec{r}_{i_{k-1}i_k}}{\left|\Delta\vec{r}_{i_k i_{k+1}}\right|\left|\Delta\vec{r}_{i_{k-1}i_k}\right|}\right) \quad (7)$$

were $\phi_{critical}$ is a critical threshold curvature angle and $f(\phi)$ is a curvature function. Otherwise stated, in this study we will choose $\phi_{critical}=\pi/2$ and $f(\phi)=1$, which is equivalent to allow only those trajectories with curvature angles smaller than 90°.

In order to illustrate formulation (6), Fig. 4 shows a hypothetical 2D graph. Probability of path ρ_2 is zero because it has a curvature in one of its nodes that exceed the critical angle $\phi_{critical}$, and therefore the path ρ_1 is more reliable than ρ_2.

The estimated nervous fiber trajectory running from $\vec{r}_s$ to $\vec{r}_p$ will be given by the most reliable path:

$$\tilde{\rho}_{s\ldots p} = \underset{\forall_{\rho_{s\ldots p}}}{\operatorname{argmax}}\left(P[\rho_{s\ldots p}]\right). \quad (8)$$

To solve Eq. (8) we propose an iterative algorithm (see Appendix A), which is an adaptation of the Moore and Dijstra algorithm (Dijkstra, 1959; Moore, 1959; Gondran and Minoux,

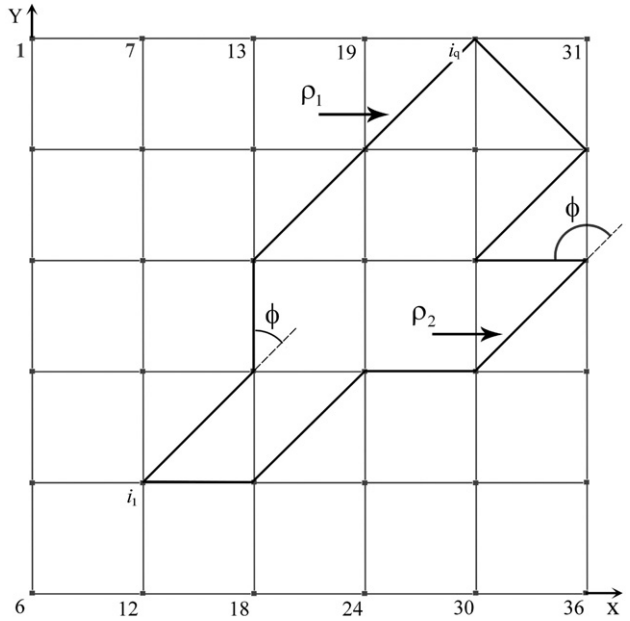

Fig. 4. Hypothetical simple 2D graph. The set of 36 nodes is consecutively enumerated, the nodes i_1=11 and i_q=25 in the figure are linked by two paths $\rho_1(\vec{r}_{i_1},\vec{r}_{i_q})$ and $\rho_2(\vec{r}_{i_1},\vec{r}_{i_q})$. For path $\rho_1(\vec{r}_{i_1},\vec{r}_{i_q}) = \{u(\vec{r}_{i_1},\vec{r}_{i_2}); u(\vec{r}_{i_2},\vec{r}_{i_3}); \ldots; u(\vec{r}_{i_{q-1}},\vec{r}_{i_q})\}$ the sequence of nodes i_1, i_2, … , i_{q-1}, i_q is 11, 16, 15, 20, and 25. For $\rho_2(\vec{r}_{i_1},\vec{r}_{i_q})$ the sequence is: 11, 17, 22, 28, 33, 27, 32 and 25. The probability of path ρ_2 is null, $P[\rho_2\ (r_{i_1}, r_{i_q})]=0$, because this path has a curvature in node 33 that exceeds the critical angle $\phi_{critical}=\frac{\pi}{2}$. In particular $\phi = \arccos\left(\frac{\Delta\vec{r}_{i_5,i_6},\Delta\vec{r}_{i_4,i_5}}{|\Delta\vec{r}_{i_5,i_6}||\Delta\vec{r}_{i_4,i_5}|}\right) = \frac{3\pi}{4}$, where i_4=28, i_5=33 and i_6=27. In this case path ρ_1 is more probable than ρ_2.

1984) to solve the shortest path problem in a graph. The resulting map $M(\vec{r}_s,\vec{r}_p)$ is the probability of the path between nodes $\vec{r}_s$ and $\vec{r}_p$ of maximum reliability, which is the solution of Eq. (8).

In general, the anatomical connectivity between nodes $\vec{r}_s$ and $\vec{r}_p$ can be defined as a function 'g' of the arc weights of $\tilde{\rho}_{s\ldots p}$ and the a priori term $C_{prior}(\vec{r}_s,\vec{r}_p)$:

$$C_{node}(\vec{r}_s,\vec{r}_p) = g\big(w(a_{s\ i_2}),\ldots,\ w(a_{i_{L-1}p}),\ C_{prior}(\vec{r}_s,\vec{r}_p)\big), \tag{9}$$

$C_{prior}(\vec{r}_s,\vec{r}_p)$ represents the a priori information about the connectivity between nodes $\vec{r}_s$ and $\vec{r}_p$, which could come from histological tracing methods or other neuroimaging techniques (e.g. fMRI, EEG/MEG tomography, PET, etc.). When there is not prior information available, $C_{prior}(\vec{r}_s,\vec{r}_p)$ may be a non-informative prior or not evaluated at all, as will be the case in this work.

A straightforward definition of the function 'g' could be $M(\vec{r}_s,\vec{r}_p)$. However, this measure decreases strongly with the path longitude, stating a high contrast in connectivity values between pairs of near and distant nodes. In this work, similarly to Parker et al. (2002) and Staempfli et al. (2006), the anatomical connectivity measure is defined as the lowest weight of the arcs belonging to the most probable path, i.e. 'g' is the minimum function and equation (9) becomes:

$$C_{node}(\vec{r}_s,\vec{r}_p) = \min_{\forall a\in\tilde{\rho}_{s\ldots p}}(w(a)). \tag{10}$$

Zone-zone connectivity

In the graph framework presented here, the evaluation of connectivity between clusters of nodes in G_{brain} will be used for defining of connectivity measures between brain anatomical areas.

Let the graph $G_{brain}=[N,A]$ be redefined as a $K+1$ partite undirected graph where the nodes set N is partitioned in K non-overlapped gray matter subsets N_k, $k=1,\ldots,K$, and one subset N_{rest} clustering all voxels not belonging to brain gray matter (i.e. cerebral spinal fluid and white matter). The K gray matter clusters represent the anatomical areas, denoted by $A_1,\ldots,A_K$. Generally those areas are segmented based upon cytoarchitectonic, histological or other sort of anatomic and functional information (e.g. Broadmann areas) through manual, automatic or semi automatic procedures.

In this context the arcs are defined directly between nodes of different areas. The term $a_{ij}(\vec{r}_m,\vec{r}_n)$ represents the arc that links node $\vec{r}_m\in N_i$ with node $\vec{r}_n\in N_j$. The weight of this arc $\omega(a_{ij}(\vec{r}_m,\vec{r}_n))$ will be a function of the node–node connectivity measure defined previously by Eq. (10). This can be expressed in general by the following formula:

$$\omega(a_{ij}(\vec{r}_m,\vec{r}_n) = h\big(C_{node}(\vec{r}_m,\vec{r}_n),\ P_i(\vec{r}_m),\ P_j(\vec{r}_n)\big). \tag{11}$$

This expression also includes the uncertainty of each node $\vec{r}_s\in N_{\bar{k}}$ to be a member of its anatomical area $\bar{k}$ through a probability term $P_{\bar{k}}(\vec{r}_s)$. This probability comes from a Maximum Probability Segmentation Map (Mazziotta et al., 1995), which means that $P_{\bar{k}}(\vec{r}_s) = \max_{k=1..K}(P_k(\vec{r}_s))$.

Particularly, for the sake of simplicity, we will assume the following expression for the weight of the arc:

$$\omega(a_{ij}(\vec{r}_m,\vec{r}_n)) = C_{node}(\vec{r}_m,\vec{r}_n)P_i(\vec{r}_m)P_j(\vec{r}_n). \tag{12}$$

Additionally, it is necessary to define a subdivision of each cluster N_k into a boundary nodes set N_k^s and a core nodes set N_k^c, such that $N_k^s\cup N_k^c=N_k$. The boundary nodes set N_k^s comprises those voxels having at least one neighbor that does not belong to N_k. Finally, a general definition for zone–zone connectivity is established as:

$$C_{zone}(A_i,A_j) = t\big(\omega(a_{ij}(\vec{r}_m,\vec{r}_n)),C_{prior}(A_i,\ A_j)\big) \tag{13}$$

for all $\vec{r}_m\in N_i$ and $\vec{r}_n\in N_j$. Similar as in Eq. (9), the term $C_{prior}(A_i, A_j)$ represents the a priori information about the connection between areas A_i and A_j.

The general zone-zone connectivity measure (13) can be reasonably restricted to white matter connections. This is accomplished by taking into account only connectivity between voxels of the surface of the corresponding anatomical areas, since voxels in the core nodes set N_k^c belong to gray matter and connections to (and among) them are beyond the scope of the present methodology. Based on this, we introduce three different anatomical connectivity measures, namely: Anatomical Connection Strength (ACS), Anatomical Connection Density (ACD) and Anatomical Connection Probability (ACP). Let us explain each in detail:

- ACS is required to be a measure of the potential information flow between the connected areas A_i and A_j. This would be related to the cross sectional area of the fiber bundle connecting the surfaces of the zones, which will give an estimate of the amount of nervous fibers shared by these areas. Therefore, we propose to estimate the ACS by counting the nodes on the surface of A_i and A_j involved in the connection, where each node is weighted by its anatomical connectivity value with the surface of the second zone. The connectivity value of node $\vec{r}_n\in N_j^s$ will be denoted as $\zeta_{\vec{r}_n}\big(0\le\zeta_{\vec{r}_n}\le1\big)$ and defined as the maximum arc weight among all connections between $\vec{r}_n$ and any $\vec{r}_m\in N_i^s$:

$$\zeta_{\vec{r}_n} = \max_{\forall\ \vec{r}_m\in N_i^s}\big(\omega(a_{ij}(\vec{r}_n,\vec{r}_m))\big). \tag{14}$$

  Then, the final expression for the ACS reads:

$$C_{Zone}^{ACS}(A_i,A_j) = \sum_{\forall\vec{r}_m\in N_i^s}\zeta_{\vec{r}_m} + \sum_{\forall\vec{r}_n\in N_j^s}\zeta_{\vec{r}_n}, \tag{15}$$

  where we have explicitly written two terms, one quantifying connections of the region A_i with A_j, and the other quantifying connections of the region A_j with A_i.
- ACD is searched as a measure of the fraction of the surface involved in the connection with respect to the total surface of both areas. Thus, it can be estimated as the ACS relative to the number of nodes belonging to the surfaces of A_i and A_j:

$$C_{Zone}^{ACD}(A_i,A_j) = \frac{C_{Zone}^{ACS}(A_i,A_j)}{|N_i^s|+|N_j^s|}. \tag{16}$$

- ACP is searched as a measure of the probability of two areas to be connected at least by a single connection. Then, we define it as the maximum connectivity value between nodes of areas A_i and A_j:

$$C_{Zone}^{ACP}(A_i,A_j) = \max\left(\max_{\forall\vec{r}_m\in N_i^s}\zeta_{\vec{r}_m},\max_{\forall\vec{r}_n\in N_j^s}\zeta_{\vec{r}_n}\right). \tag{17}$$

Experimental data

Artificial data

Diffusion tensor phantom simulated data sets were obtained from the Centre for Neuroimaging Sciences, Institute of Psychiatry, King's College London. The DW-MRI data were simulated using a spin-echo sequence with the following parameters: 30 diffusion encoding directions (Jones et al., 1999); $b=1000$ s/mm^2; image resolution $2\times2\times2$ mm^3; TE=160 ms. T2 values for the tract and background were assumed to be the same as white matter (65 ms) and grey matter (95 ms) at 1.5 T, respectively. Three data sets are available with varying levels of SNR (7, 15 and 31).

Three out of ten different tract configurations were selected to evaluate the performance of the proposed methodology (see Fig. 5): straight crossing, curved crossing and the tract inspired in the maple leaf (Feuille trajectory). For each of them, the six diffusion elements, the eigenvectors and the corresponding T2-weighted images for each SNR data set were provided. The corresponding ODF maps were estimated using a simple procedure described in Appendix B. A threshold value was applied to the T2-weighted image in order to create a binary mask (P_{mat}) expressing the presence or not of gray/white matter tissue.

Additionally, two other artificial diffusion data sets were created using the following geometric parameters: $55\times55\times55$ voxels; image resolution $2\times2\times2$ mm^3. The first artificial data set represents a branching fiber tract (Fig. 6a). In branching areas, the first and second eigenvalues of the diffusion tensor were assumed to be equal (i.e. oblate tensor). The second artificial data set represents a fiber crossing of three orthogonal tracts (Fig. 6b). In crossing areas, the three tensor's eigenvalues were assumed to be approximately the same (i.e. spherical tensor). In both configurations, three different SNR (7, 15 and 31) were considered to create the diffusion tensor elements. ODF maps were estimated using the procedure described in Appendix B.

Human data

Using a standard diffusion gradient direction scheme (twelve diffusion-weighted images and a $b=0$ image), DW-MRI data were acquired from 5 healthy subjects using a MRI scanner Siemens Symphony 1.5 T (Erlangen, Germany) and a single shot EPI sequence. To each subject, two interleaved sets of 25 slices of 6 mm thickness with a distance factor of 100% were acquired with the following parameters: $b=1200$ s/mm^2; FOV=256×256 mm^2; acquisition matrix=128×128; corresponding to an 'in plane' spatial resolution of 2×2 mm^2; TE/TR=160 ms/7000 ms. Two interleaved sets were necessary because it was impossible to cover the whole head with a good spatial resolution using a single set due to a pulse sequence limitation (max: 35 slices). Both sets were joined to form a volume of 50 contiguous slices of 3 mm thickness covering the whole brain for each subject. The aforementioned acquisition was repeated 5 times to improve signal to noise ratio (SNR). In order to improve EPI quality, magnitude and phase difference images of a T2 gradient echo field mapping sequence were acquired with TE=7.71 ms and 12.47 ms.

Also, a 3D high resolution T1-weighted image (MPRAGE) covering the whole brain was acquired with the following parameters: 160 contiguous slices of 1 mm thickness in sagittal orientation; in plane FOV=256×256 mm^2, corresponding to an in plane spatial resolution of 1×1 mm^2; TE/TR=3.93 ms/3000 ms.

Although the scanner sequence performs an eddy current automatic correction, in order to remove remaining distortions an affine 3D mutual normalized information-based registration method (Studholme et al., 1998) was used. The DW-MRI images were attempted to be corrected from EPI distortions using the SPM FieldMap toolbox (Hutton et al., 2002).

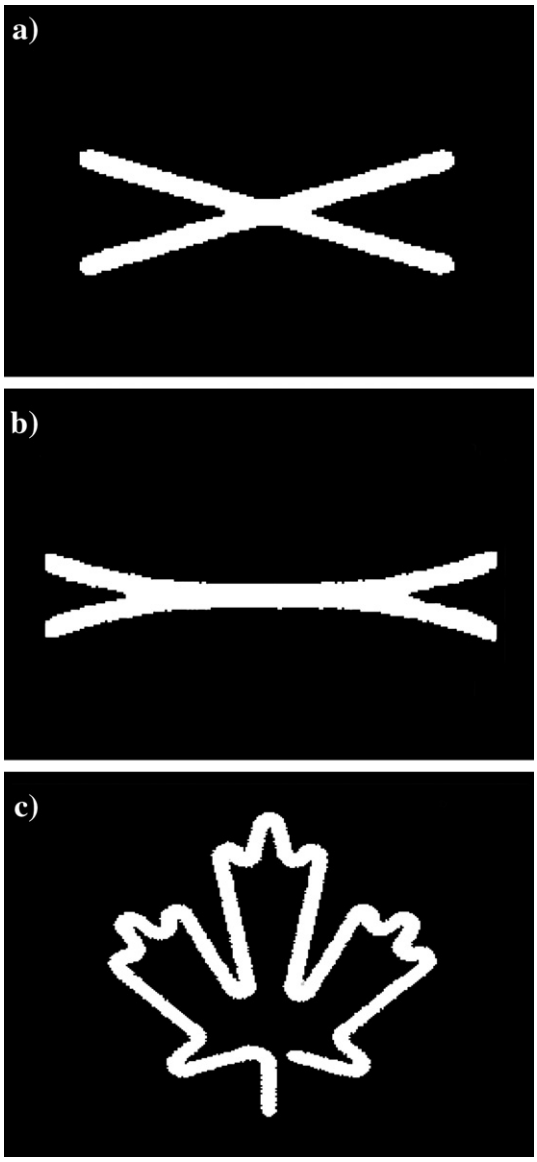

Fig. 5. Phantom tract configurations obtained from the Centre for Neuroimaging Sciences, Institute of Psychiatry, King's College London (http://neurology.iop.kcl.ac.uk/dtidataset/Common_DTI_Dataset.htm). The configurations used in this study were: (a) straight crossing, (b) curve crossing, and (c) tract inspired in the maple leaf (Feuille trajectory).

T1-weighted 3D anatomical image was registered to the $b=0$ image using a normalized mutual information method (Studholme et al., 1998). Using the SPM2 toolbox (available at http://www.fil.ion.ucl.ac.uk/spm/software/spm2), a low dimensional normalization (Ashburner and Friston, 1999) to a stereotaxic space MNI (Evans and Collins, 1993) was estimated for the registered T1-weighted image, which was written with an spatial resolution of $2\times2\times2$ mm^3. Employing the aforementioned transformation, DW-MRI data were fitted to a diffusion tensor (Basser et al., 1994) in each voxel of the stereotaxic space. Tensors were rotated

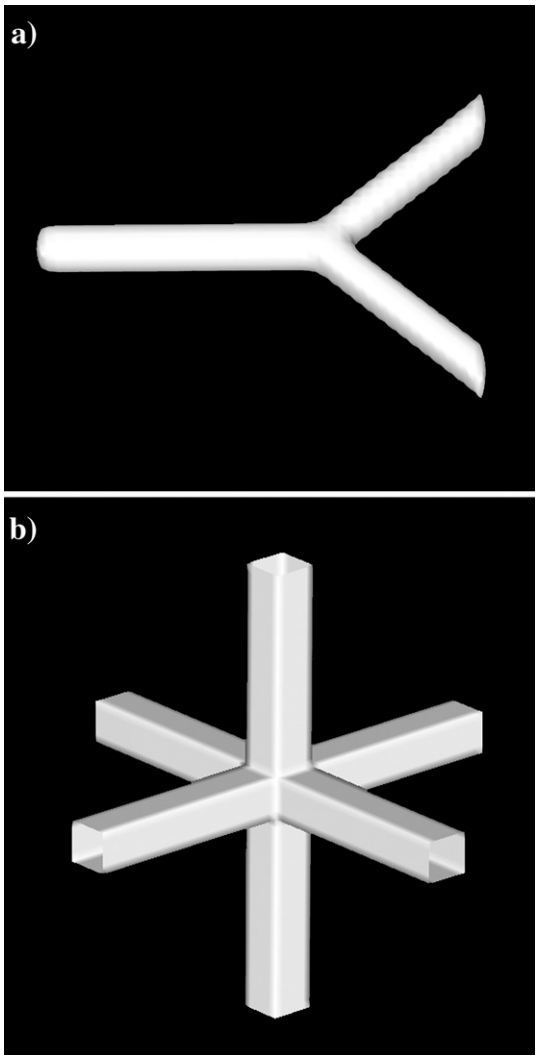

Fig. 6. Additional artificial tract configurations created to explore the performance of the proposed methodology. (a) Branching fiber tract. (b) Fiber crossing of three orthogonal tracts.

according to the method presented by Alexander and coworkers (Alexander et al., 2001).

Probabilistic tissues segmentations of gray matter, white matter and cerebral spinal fluid (Ashburner and Friston, 2000) were obtained from the normalized T1-weigthed image using the SPM2 toolbox. The gray and white matter segmentation probabilistic maps (P_{GM} and P_{WM}, respectively) were used to construct the anatomical information function P_{mat} evaluating Eq. (3), with $\alpha=1$. Also, the normalized T1-weigthed image was automatically segmented into 71 gray matter structures using the IBASPM toolbox (available at http://www.fil.ion.ucl.ac.uk/spm/ext/#IBASPM) (Alemán-Gómez et al., 2006) and the average Probabilistic MRI Atlas created by the Montreal Neurological Institute (Collins et al., 1994; Evans et al., 1994). For evaluating the arcs weight in expression (11), the probability of each voxel $\vec{r}_s \in N_k$ to belong to k-th anatomical area was set to unity ($P_k(\vec{r}_s)=1$), although as it was mentioned in Section 2.4, this probability can be more realistically evaluated employing Maximum Probability Segmentation Maps (Mazziotta et al., 1995). Again, the ODF maps were estimated using the procedure described in Appendix B.

Results

Artificial data

The performance of the proposed methodology was explored using artificial DW-MRI data. Firstly, anatomical connections between different regions of interest (ROIs), defined for the straight crossing, curve crossing and Feuille trajectory were estimated (see Fig. 7). Each ROI consists of seven contiguous voxels representing a line perpendicular to the fiber tract being analyzed. Left column (Figs. 7a, c and e) shows the reconstructed connection routes (most probable paths) between ROI1 and the others, with SNR level of 15. These results illustrate the ability of our method to reconstruct complex fiber tracts configurations (see for example the Feuille trajectory results, Fig. 7e). Complementarily, right column (Figs. 7b, d and f) shows the corresponding maximum voxel–voxel connectivity values with ROI1 (i.e. each voxel of the image volume was assigned its maximum voxel–voxel connectivity value with the voxels of ROI1). Note that, although for the straight crossing and curve crossing the method provides anatomical connection routes between ROI1 and ROI4, the corresponding voxel–voxel connectivity values indicate the low probability of connection between these ROIs, which is in accordance with the characteristics of the tracts configurations. In contrast, the obtained voxel–voxel connectivity values between ROI1–ROI2 and ROI1–ROI3 indicate the high probability of connection between these ROIs.

Secondly, we analyzed the branching configuration shown in Fig. 6a. Both Fig. 8 and Table 1 show the results before and after a hypothetical loss of the white matter integrity. Three different ROIs were defined (Fig. 8a): ROI1 consists of two contiguous voxels at the left end of the fiber tract, ROI2 consists of four contiguous voxels at the upper right end of the tract and ROI3 is conformed by a single voxel at the bottom right end of the tract. For simulating a hypothetical loss of the white matter integrity (hereinafter, WM-affectation, for brevity), the values of two voxels in the binary mask (P_{mat}) were set to zero (each voxel located symmetrically at the upper right tract or at the bottom right tract, see Fig. 8b). Figs. 8c and d correspond to the maximum voxel–voxel connectivity values between the voxels of ROI1 and the rest of voxels before and after the WM-affectation, respectively. Also, Table 1 helps us to understand the interrelationship between the ACS, ACD and ACP measures and their sensitivity to white matter affectation. For example, note that before WM-affectation the C^{ACS}_{Zone} (ROI1, ROI2) is around twice the C^{ACS}_{Zone} (ROI1, ROI3) since the total number of superficial voxels in ROI1 and ROI2 duplicates the total number of superficial voxels in ROI1 and ROI3 (i.e. 6 and 3 voxels, respectively). However, C^{ACD}_{Zone} (ROI1, ROI2) and C^{ACD}_{Zone} (ROI1, ROI3) are similar and the small difference between them can be explained by the different geometrical characteristics of the defined ROIs. In this case, both ROI2 and ROI3 present very high probabilities of connection with ROI1 for all SNR levels. After the WM-affectation, these probabilities of connection as well as the ACS and ACD measures decrease considerably.

Finally, the performance of our model in comparison with SLT and aFM methods was studied in the case of fiber crossing of three orthogonal tracts, as shown in Fig. 9. Starting and ending ROIs were defined as planes of 5×5 voxels (i.e. each ROI containing 25 voxels) at the two ends of the fiber tract being analyzed. Most of the fiber paths generated from ROI1 using SLT method terminate in the crossing fiber region or go to the perpendicular tracts (Fig.

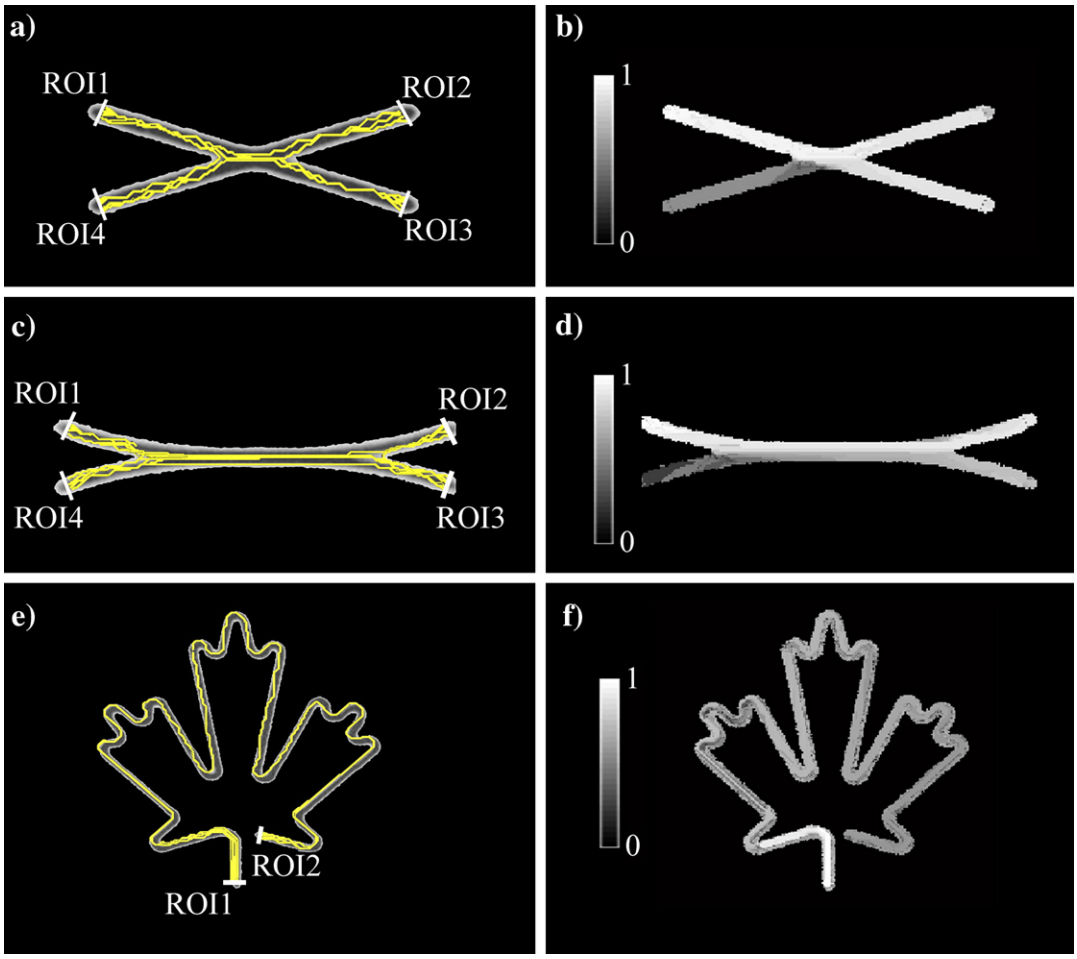

Fig. 7. Resulting anatomical connections between different regions of interest (ROIs) defined for straight crossing, curve crossing and Feuille trajectory. Each defined ROI consists of seven contiguous voxels defining a perpendicular line to the corresponding fiber tract. Left column (Figs. 7a, c and e): reconstructed connection routes (most probable paths) between ROI1 and the other defined ROIs, with SNR level of 15. Right column (Figs. 7b, d and f): corresponding maximum voxel–voxel connectivity values between the image volume voxels and the ROI1 voxels. The color code represents the index of connectivity. (For interpretation of the references to colour in this figure legend, the reader is referred to the web version of this article.)

9a). In contrast, both aFM and our graph-based tractography method reconstructed tracts between ROI1 and ROI2 (Figs. 9b and c, respectively). However, some fiber paths found by aFM failed to follow the correct fiber tract (e.g. some of them strayed from the fiber tract being analyzed at the level of the crossing region, going to the other perpendicular tracts and doing a U-turn before coming back to the main fiber to eventually reach the ending ROI).

Complementarily, Table 2 presents the obtained ACS, ACD and ACP measures using aFM and the proposed approach. Notice that although the zone–zone connectivity measures were not defined in the aFM, we used the voxel–voxel connectivity provided by this method to evaluate Eqs. (15), (16) and (17). The resulting C^{ACP}_{Zone} (ROI1, ROI2) using aFM is lower than that provided by our approach. Similarly, C^{ACS}_{Zone} (ROI1, ROI2) and C^{ACD}_{Zone} (ROI1, ROI2) measures for the aFM method are more distant from their ideal values (50 for the ACS, and 1 for the ACD measure).

It is interesting to note that in this experiment, the fiber paths obtained by our method look rougher or noisier (i.e. changing directions from voxel to voxel) inside the crossing region (Fig. 9c). This effect is explained by the fact that in this region the diffusion tensor is nearly spherical, and any fiber tracking method relying on estimating an ODF will be affected by the goodness of this estimation. In this work, the ODF is estimated from the Diffusion tensor model (Appendix B). This is a very simple method which is usually not able to describe complex fiber configurations, as is the case in crossing regions. In the Summary and discussions section the advantages of using more advanced models to infer the ODF will be illustrated.

Human data

In order to explore the performance of the proposed method in real data, we tried to replicate three well known brain anatomical connections. First, anatomical connections between voxels of the occipital pole surfaces (OCCs) and voxels belonging to the white matter and to the gray matter regions surfaces (WM-GMs) were estimated. The reconstructed connection routes (most probable paths) between left and right OCCs are shown in Fig. 10a. Figs. 10b and c show axial maps of the node–node connectivity values at the level of the splenium of the corpus callosum and the lateral geniculate nucleus, respectively. In these maps, each voxel was assigned the maximum of all possible connectivity values between it and the voxels of both OCC areas. Fig. 10a illustrates how the connection routes pass correctly through the splenium of the corpus

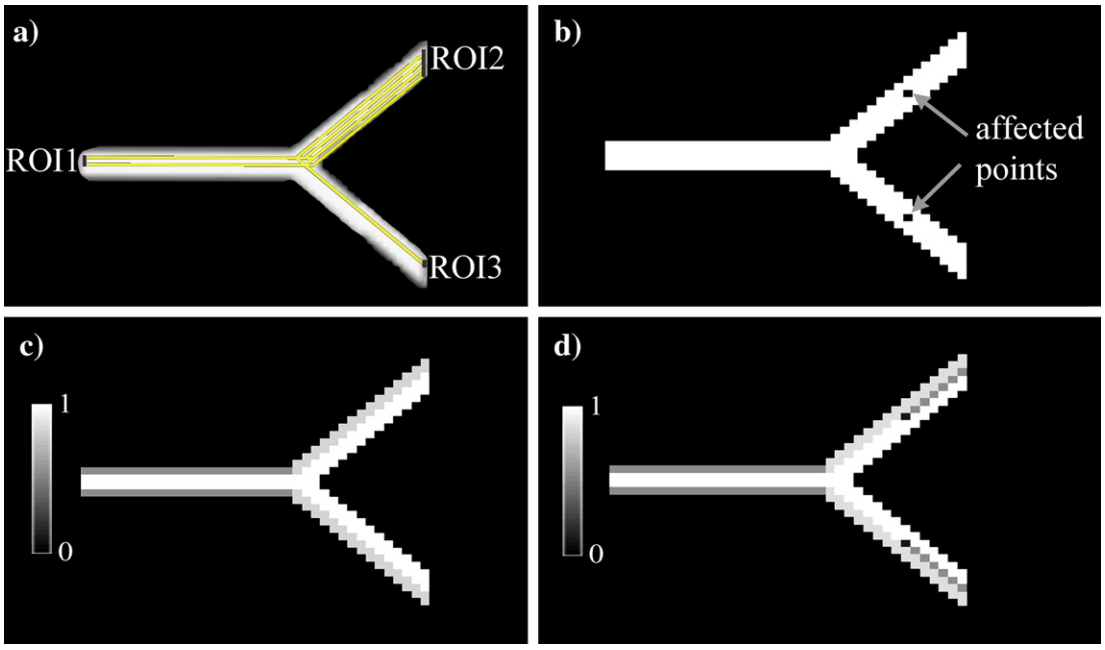

Fig. 8. Anatomical connections for the branching configuration before and after a hypothetical loss of the white matter integrity. (a) Three different ROIs were defined: ROI1 consists of two contiguous voxels at the left end of the fiber tract, ROI2 consists of four contiguous voxels at the upper right end of the tract, and ROI3 is conformed by a single voxel located at the bottom right end of the tract. Reconstructed connection routes (most probable paths) between ROI1–ROI2 and ROI1–ROI3 are also represented. (b) To simulate a hypothetical loss of the white matter integrity, the values of two voxels in the binary mask (P_{mat}) were set to zero (each voxel located symmetrically at the upper right tract or at the bottom right tract). (c) Obtained maximum voxel–voxel connectivity values between the image volume voxels and the ROI1 voxels before the hypothetical loss of the white matter integrity. The color code represents the index of connectivity. (d) Similar to (c), but after the hypothetical loss of the white matter integrity. (For interpretation of the references to colour in this figure legend, the reader is referred to the web version of this article.)

callosum and Figs. 10b and c confirm the expected high connectivity values for this region and the optic radiation, respectively. These results are in accordance with existing anatomical knowledge (Gómez-Padrón et al., 1985; Witelson, 1989; Standring, 2004).

The anatomical connections between voxels of an axial seed plane (ASP) placed in the corticospinal tract at the level of the pons (which is considered as a region) and voxels belonging to the WM-GMs were also estimated. Fig. 10d shows the reconstructed routes connecting the ASP and the left and right postcentrals gyrus, passing through the internal capsule. Moreover, Figs. 10e and f illustrate how regions of highest connectivity belong to the internal capsule, the corona radiata and the motor cortex (Gómez-Padrón et al., 1985; Standring, 2004).

Table 1
Results for branching configuration using the proposed connectivity graph model

SNR	C^{ACS}_{Zone} (ROI1, ROI2)	C^{ACS}_{Zone} (ROI1, ROI3)	C^{ACD}_{Zone} (ROI1, ROI2)	C^{ACD}_{Zone} (ROI1, ROI3)	C^{ACP}_{Zone} (ROI1, ROI2)	C^{ACP}_{Zone} (ROI1, ROI3)
Connectivity measures in branching configuration						
7	5.56	2.60	0.92	0.87	0.99	1
15	5.57	2.58	0.92	0.86	0.99	0.99
31	5.58	2.59	0.93	0.86	1	1
Connectivity measures after affecting the white matter mask						
7	3.98	1.58	0.66	0.52	0.98	0.59
15	3.96	1.57	0.66	0.52	0.99	0.59
31	3.96	1.57	0.66	0.53	0.99	0.60

In a similar way, anatomical connections between voxels of the middle frontal gyrus (MFGs) and the WM-GMs voxels were estimated (see Figs. 10g–i). We tried to obtain the fibers trajectories first between the thalamus and the MFGs, and finally between the left and right MFGs. In both cases, the main difficulty lies in the fact that the connecting fibers should pass through the crossing of three major bundles (i.e. intersection of the superior longitudinal fasciculus, the corona radiata and the corpus callosum). Note that the obtained routes connecting the thalamus and the MFGs (Fig. 10g) pass through the internal capsule and the corona radiata in accordance with previous anatomical studies (Gómez-Padrón et al., 1985; Standring, 2004). Also, those connection routes between the left and right MFGs (Fig. 10g) pass specifically through the genu and the rostral body of the corpus callosum and Figs. 10h and i confirm the expected high connectivity values for these regions, agreeing with Witelson's corpus callosum subdivision (Witelson, 1989).

Fig. 11 shows the mean ACS, ACD and ACP maps between 71 brain gray matter regions for five healthy subjects. For each subject, ACS, ACD and ACP measures were computed after eliminating not significant connectivity values between the WM-GMs voxels and the set of defined gray matter structures. Significant values were found by a z-test (H_0: $z \leq 0$) with a 0.05 significance level. In each map, the element $C_{i,j}$ is the mean connectivity value between regions i and j. Note that as we defined non-directed ACS, ACD and ACP measures, the resulting maps are symmetrical. Also, it can be spotted 2 black lines (4 with the symmetry) in all maps. These correspond with the left and right subthalamic nucleus, which were not correctly defined by the automatic parcellation method due to their very small sizes.

According to the mean ACS map (Fig. 11a), the precentral gyrus left and the postcentral gyrus left are the most connected regions (i.e. they present the maximum ACS value, 387.16± 97.87). These regions play an important role in a wide variety of the brain functions (e.g. motor and somatosensory functions). In general, frontal and temporal structures are the most connected structures. On the other hand, the most densely connected regions are the caudate nucleus right and the thalamus right (connecting around the 10±3% of their surfaces). It is known that the caudate nucleus is involved in the control of voluntary movement and in learning and memory systems. Taking into account the mean ACP map (Fig. 11c), the average connection density (i.e. the number of all non-zero connections divided by the maximum possible number of connections) was 0.7. This means that about the 70% of all possible connections between any two of the defined brain structures have a non-zero probability.

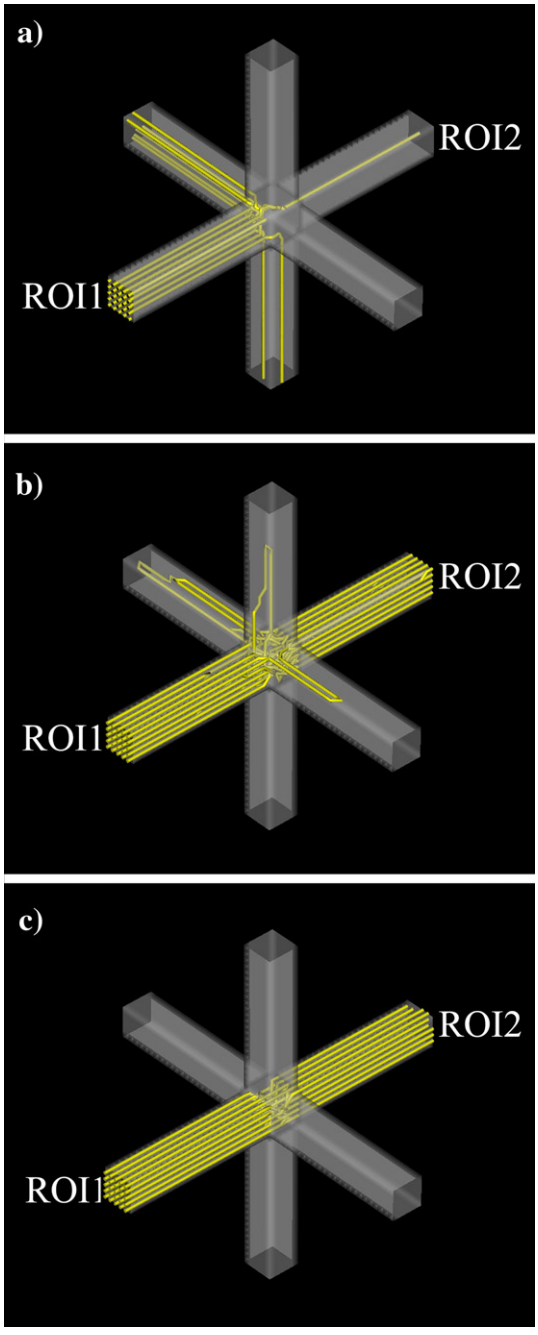

Fig. 9. Tracking results for the fiber crossing of three orthogonal tracts with SNR level of 15. ROI1 and ROI2 were defined as planes of 5×5 voxels at the two ends of the fiber tract being analyzed. (a) All paths generated from ROI1 using the SLT method. (b) Obtained connection routes between ROI1 and ROI2 using the aFM method. (c) Obtained connection routes between ROI1 and ROI2 using the proposed methodology.

Table 2
Results for orthogonal crossing of three fiber tracts using aFM and the proposed connectivity graph model

Connectivity measures in orthogonal crossing using aFM and the connectivity graph model

SNR	aFM			Graph model		
	C^{ACS}_{Zone} (ROI1, ROI2)	C^{ACD}_{Zone} (ROI1, ROI2)	C^{ACP}_{Zone} (ROI1, ROI2)	C^{ACS}_{Zone} (ROI1, ROI2)	C^{ACD}_{Zone} (ROI1, ROI2)	C^{ACP}_{Zone} (ROI1, ROI2)
7	23.53	0.47	0.50	36.41	0.72	0.90
15	23.80	0.48	0.50	37.78	0.76	0.91
31	24.63	0.49	0.51	42.73	0.85	0.98

In order to evaluate (dis)similarity between the different subjects, correlation coefficients between their corresponding ACS, ACD and ACP maps were estimated (see Table 3). Results show significant correlations in all cases (the maximum p value obtained was in the order of 10^{-209}), supporting the hypothesis that healthy subjects present similar ACS, ACD and ACP patterns for the gray matter parcellation used in this study.

Summary and discussions

In this work, we developed a diffusion imaging methodology capable to characterize anatomical connections between different brain gray matter structures. It consists of three basic steps: 1, definition of a Brain Graph model in which each voxel is considered as a node of a non-directed weighted graph; 2, the use of an iterative algorithm based on analysis of the voxels neighborhood to find the route of maximum probability between two nodes and the subsequent definition of the anatomical connectivity measure between them; 3, the definition of three anatomical connectivity measures between different gray matter regions, which are individually considered as clusters of nodes in the graph.

In step 1, the probabilistic tissue segmentation of the anatomical MR image and the intravoxel white matter orientational distribution function (ODF), obtained from DW-MRI, are combined to estimate the probability of nervous fibers connection between two contiguous nodes (voxels), which is associated to the weight of the arc connecting these nodes.

Generally, in the diffusion tracking framework, the fractional anisotropy (FA) map is used to construct a binary mask which is employed to constraint the fiber trajectories space (Conturo et al., 1999; Mori and van Zijl, 2002; Staempfli et al., 2006). Assuming that nervous fibers are present only in those regions with high anisotropy, this mask is defined by an empirical threshold on the FA map, which implies that regions where two or more fibers cross each other will be ignored. To our knowledge, this work introduces for the first time, the use of probabilistic brain tissue segmentations of the anatomical MR images as a priori information to find anatomically plausible connection routes between any two voxels.

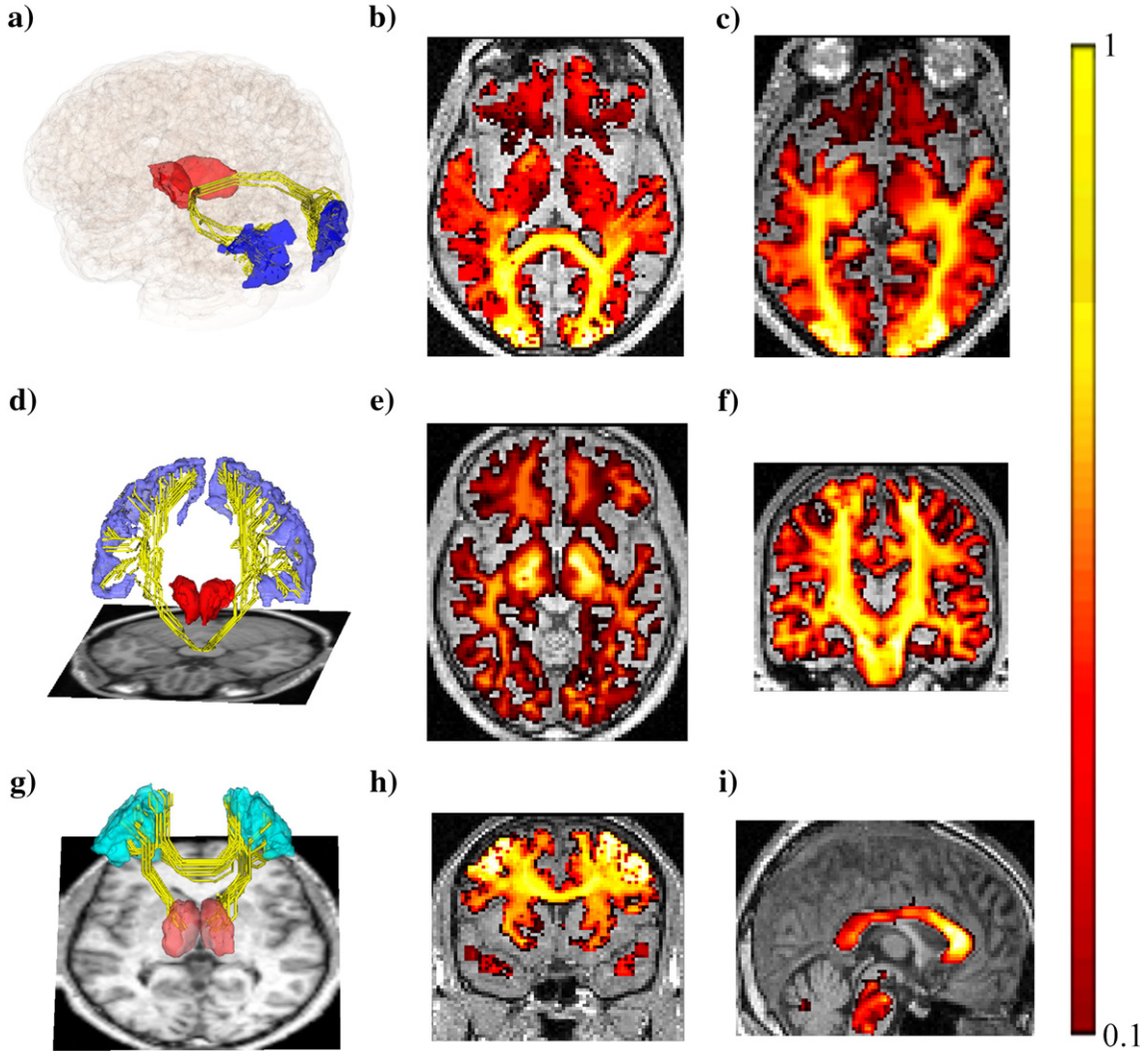

Fig. 10. (a) Obtained anatomical connection routes between the left and right occipital poles. Both thalami are represented as anatomical references. (b) Axial map at the level of the splenium of the corpus callosum representing maximum voxel–voxel connectivity values between the WM-GMs voxels and the OCCs voxels. (c) Axial map at the level of the lateral geniculate nucleus representing maximum voxel–voxel connectivity values between the WM-GMs voxels and the OCCs voxels. (d) Reconstructed connection routes between the ASP and the left and right postcentral gyrus. (e) Axial map representing maximum voxel–voxel connectivity values between the WM-GMs voxels and the voxels of the ASP. (f) Coronal map representing maximum voxel–voxel connectivity values between the WM-GMs and the ASP voxels. (g) Obtained connection routes among the left and right MFGs, and between each MFGs and the ipsilateral thalamus. (h) Coronal map representing maximum voxel–voxel connectivity values between the WM-GMs voxels and the MFGs voxels. (i) Inter-hemispheric plane representing maximum voxel–voxel connectivity values between the WM-GMs voxels and the MFGs voxels. In (b), (c), (e), (f), (h) and (i) the color code represents the index of connectivity. Each connectivity map was overlaid on the corresponding T1-weighted image. (For interpretation of the references to colour in this figure legend, the reader is referred to the web version of this article.)

Additionally, we allow for tuning the relative importance between the probabilistic gray and white matter segmentations through the α parameter (see Eq. (3)). For $\alpha \geq 1$, the segmentation of white matter will have equal or bigger weight than the gray matter segmentation, which agrees with the fact that nervous fibers are mostly in the white matter. However, α should not be considerably greater than one (for example: $\alpha = 10$), because voxel–voxel connections around gray matter can be rejected. Thus, although in this study we chose $\alpha = 1$, the appropriate selection of this parameter requires detailed future analysis.

On the other hand, the weight of the arc connecting two neighboring nodes is defined by taking into account the fibers coherence along its direction. The probability that a fiber is present around a particular arc is evaluated by computing the integral of the ODF in a solid angle along its direction (see Fig. 3), which contributes to reduce discretization errors at the same time that complex structural fiber distributions can be considered. However, the ODF is just one of several measures that implicitly reflect fiber coherence. In this sense, the graph-based approach has the advantage that other functions can be used for this purpose, such as those characterizing fiber distribution with various maxima of orientation (Jansons and Alexander, 2003; Tuch, 2004; Alexander, 2005) or even the ellipsoids given by the diffusion tensors (Basser et al., 1994).

In order to find the anatomical connection route between two nodes in the defined Brain Graph, we explored the set of all

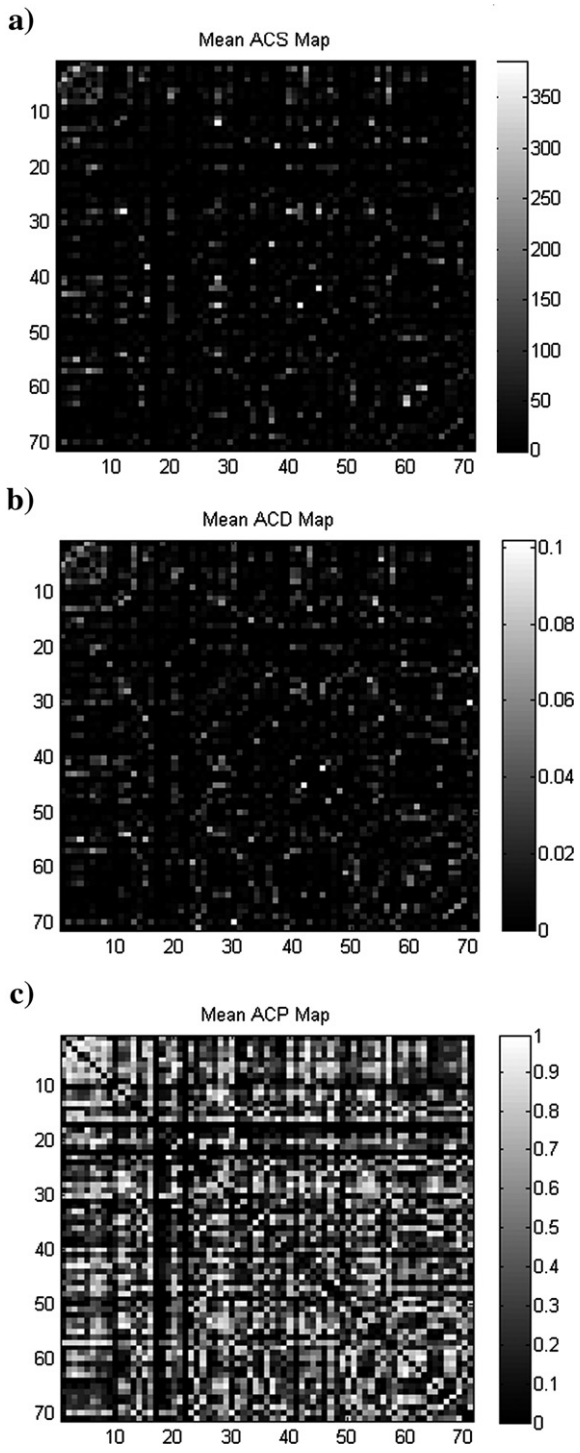

Fig. 11. Mean connectivity results for 71 gray matter regions defined on the brain of five healthy subjects: (a) ACS, (b) ACD and (c) ACP. In each map, the element $C_{i,j}$ is the mean connectivity across subjects between regions i and j. The color code represents the index of connectivity.

possible discrete paths to select the route which optimize certain function designed according to physiological criteria. A similar example of this type of procedure are the Fast Marching (FM) tractography techniques (Parker et al., 2002; Staempfli et al., 2006), in which the route connecting two voxels should minimize the "time" necessary to arrive from one voxel to the other. In our case, the fiber tractography is expressed in terms of the most probable path in the defined Brain Graph. Figs. 7–9 illustrate the performance of the proposed tractography method in the artificial DW-MRI data. The results show that the methodology we have introduced here is able to reconstruct correctly complex fiber configurations such as straight crossing, curve crossing, Feuille trajectory, branching tract and orthogonal crossing of three tracts. Also, the obtained connection routes between the left and right OCCs (Fig. 10a), the defined ASP and both postcentral gyrus (Fig. 10d), the thalamus and left and right MFGs (Fig. 10g) were presented. These results agree with existing anatomical knowledge (Gómez-Padrón et al., 1985; Witelson, 1989; Standring, 2004).

Quantification of the anatomical connectivity between two voxels can be defined according to the parameters of the connection route among them and also taking into account the a priori information about the connectivity between these voxels, which could come from previous anatomical and functional studies based on histological tracing methods or neuroimaging techniques (e.g. fMRI, EEG/MEG tomography, PET, etc.). This allows the integration between different anatomical and functional connectivity measures. In this work, similar to Parker et al. (2002) and Staempfli et al. (2006), an anatomical connectivity measure is defined as the lowest weight of the arcs set belonging to the most probable path. However, we consider that other node–node (voxel–voxel) connectivity measures should be explored.

To characterize anatomical connections between K brain gray matter structures, the previous Brain Graph was redefined as a $K+1$ partite graph by partitioning the initial nodes set in K non-overlapped gray matter subsets and one subset clustering the remaining nodes. Based on the latter, three connectivity measures were defined: Anatomical Connection Strength (ACS), Anatomical Connection Density (ACD) and Anatomical Connection Probability (ACP). ACS provides an estimation of the potential information flow between any pair of regions. It is considered

Table 3
Correlations between the ACS, ACD and ACP maps of the 5 subjects

Subject	1	2	3	4	5
ACS correlation					
1	–	0.71	0.76	0.78	0.85
2		–	0.69	0.72	0.64
3			–	0.79	0.74
4				–	0.79
5					–
ACD correlation					
1	–	0.64	0.76	0.71	0.82
2		–	0.61	0.61	0.56
3			–	0.73	0.73
4				–	0.69
5					–
ACP correlation					
1	–	0.64	0.64	0.59	0.69
2		–	0.68	0.66	0.60
3			–	0.64	0.63
4				–	0.60
5					–

For each connectivity measure, the elements above the main diagonal are the correlation coefficients.
All the correlations are significant; the maximum p value obtained was in the order of 10^{-209}.

proportional to the amount of nervous fibers shared by these regions. To estimate it we considered that, similar as in a system of tubes in which the liquids flow in one extreme of a specific tube depends on its cross section area and on the rate of liquids, the potential nervous information flow can be reflected by the cross section area of the fiber connector volume on the surfaces of the two regions. Here, the ACS is estimated by counting the "effective" number of nodes on the surfaces of the zones involved in the connection, where each node is counted according to a function which represents its anatomical connectivity value with the surface of the second zone (this function ranges between 0, no connected, and 1, completely connected). When the zones of interest present a high number of superficial nodes, the proposed ACS estimation has the inconvenient that, even if the superficial nodes of the zones are not well connected, the accumulation of a great number of small node–node connectivity values can cause a high ACS. To avoid this, it is reasonable to eliminate those node–node connections with values below a specified threshold before computing the ACS, which also contributes to eliminate the nuisance connections. Although in this work we used a z-test in order to eliminate non-significance connectivity values between the WM-GMs voxels and the set of defined gray matter structures, the selection of the threshold could be carried out using more advanced local and global thresholding models, such as local false discovery rate technique (Efron, 2004, 2005) or image thresholding based on the EM algorithm (Yakoub et al., 2006). This will be the subject of future work.

On the other hand, ACD is a measure of the fraction of the connected superficial nodes with respect to the total number of superficial nodes of both areas. It permits, for example, to know if a pair of zones has more or less density of connection than other pair of zones with different or equal number of superficial nodes. Two regions with a high ACS value (compared with the ACS between others pairs of regions) not necessarily have to present a high ACD value. This situation could take place when two regions of interest contain a high number of superficial nodes. Similarly, a pair of zones with a low ACS value can present a high ACD value, which occurs specifically when the zones contain a small number of superficial nodes (each node having an anatomical connectivity value close to 1 with the surface of the other zone).

While ACS and ACD quantify the strength and density of the possible connection respectively, ACP measures the maximum probability of two regions to be connected at least by a single connection. It allows to infer if any two gray matter regions can be functionally related independently of the strength and density of the possible connection. Additionally, other zone–zone connectivity measures can be defined and some of them could be directly formulated as the combination of the three proposed measures.

Fig. 11 show the mean maps of ACS, ACD and ACP obtained between 71 gray matter structures for five healthy subjects. Significant correlations among the connectivity matrixes of the different subjects were found (Table 3), which could support the hypothesis that healthy subjects present similar ACS, ACD and ACP patterns for the used gray matter parcellation. Before presenting the aforementioned results, the anatomical connections obtained for the branching configuration before and after a hypothetical loss of the white matter integrity were presented (Fig. 8 and Table 1), illustrating how the ACS, ACD and ACP measures reflect the white matter affectation. In a similar way, more detailed comparisons between normal and pathological ACS, ACD and ACP maps (or its combinations) could be a potential procedure to detect and diagnose pathologies causing functional cognitive deficiencies related to white matter injury, such as: Alzheimer, Schizophrenia and Dyslexia. Compared to connectivity maps of normal subjects, abnormal ones can reveal certain damage in the anatomical interconnectivity between multiple functional cognitive brain areas, allowing to find those regions that are not wired properly. Other possible application of the aforementioned connectivity maps is to use them as a priori or complementary information in brain functional connectivity studies (see for example Sotero et al., 2007).

However, the lack of information about the direction of nervous fibers in DW-MRI data hinders the possibility of distinguishing between efferent and afferent projections. Thus, in the defined non-directed weighted graph, the direction of the arcs (distinction between initial and terminal nodes) is irrelevant and making the measures ACS, ACD and ACP to be bidirectional. This constitutes an inherent important limitation of DW-MRI techniques. Nevertheless, in a previous work (Young, 1993) a connectivity matrix of the primate cerebral cortex was reported where approximately only the 15% of the total possible connections between 73 brain areas were not reciprocals.

An important element in the Brain Graph model is the voxel size of the MR images (1/resolution). Reduction of the voxel size (which can be achieved directly in the data acquisition) implies a more accurate description of the brain structure, i.e. a better characterization of the intravoxel anisotropy as well as a more reliable tissue segmentation. However, the decrease of the voxel size leads to a worse SNR and implies an increase in the computational cost of the methodology.

Other important element is the angular resolution of the diffusion weighted images. In this work, we have achieved competitive results with the use of low angular resolution data, but certainly a better performance of the methodology can be obtained using high angular resolution techniques, for example Q-ball Imaging (Tuch, 2004) and diffusion spectrum MRI (Wedeen et al., 2005). A better estimation of the ODF implies a precise characterization of the intravoxel white matter disposition and thus an accurate evaluation of the fibers coherence along arcs direction, which subsequently implies a more realistic characterization of the brain structure. In order to illustrate this, in Fig. 12 a comparison of the fiber crossing of three orthogonal tracts using the introduced graph-based tractography with ODF maps estimated from (a) the Diffusion tensor model (same results that in Fig. 9c) and (b) the Q-ball Imaging technique (Tuch, 2004) is shown. Close-ups of the fiber crossing region are shown, illustrating that the calculated routes using the Diffusion tensor model (Fig. 12a) are considerably rougher or noisier than those routes obtained using the Q-ball Imaging technique (Fig. 12b). This supports the idea that high angular resolution-based techniques allow to get better results.

The Graph Theory constitutes an ideal framework for modeling diverse system situations. Given the wide use of the graph framework in several areas of physics and mathematics, multiple problems and practical applications have been undergone. In this study, this framework is applied for the first time to the fiber tracking problem and to the subsequent quantification of the brain anatomical connections from DW-MRI data. However, open problems remain related to the recognition of false fiber trajectories and to the corresponding elimination of nuisance connections. Statistical models, in which a relative high number of subjects should be considered, can be useful to investigate the variability of the connectivity maps in order to eliminate non-significant and superfluous connections. Also, as was

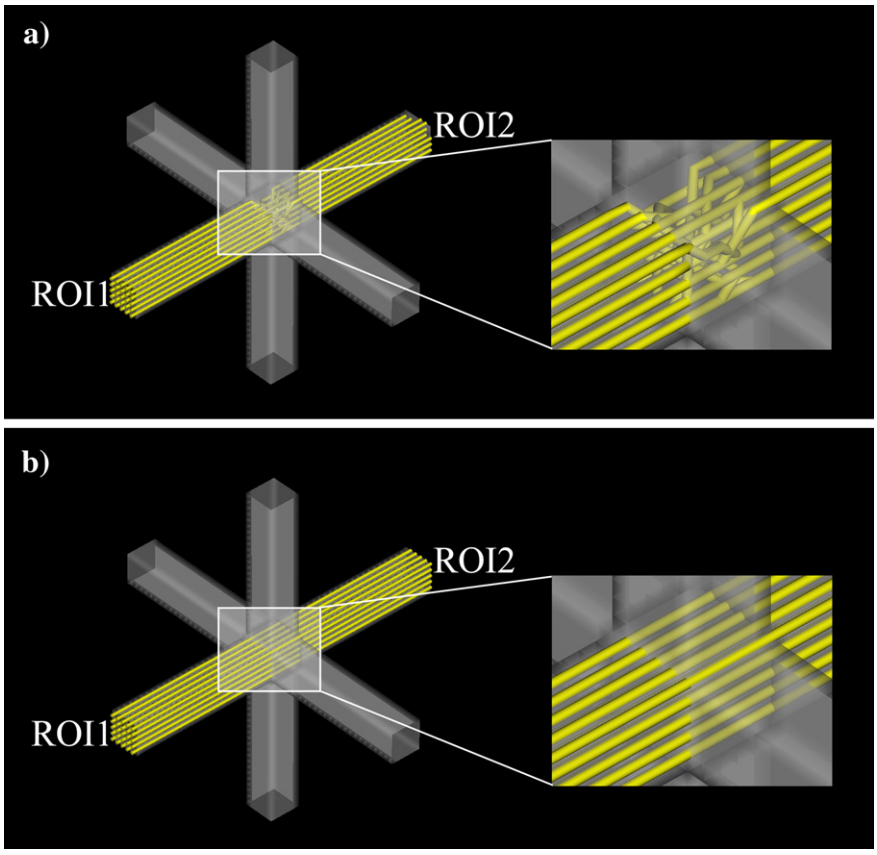

Fig. 12. Comparison of the fiber crossing of three orthogonal tracts using the graph-based tractography method with SNR level of 15 and ODF maps estimated according to: (a) Diffusion tensor model, (b) Q-ball Imaging technique. Close-ups of the fiber crossing region are shown.

mentioned in Section 2.4, the probability that a node belongs to a given gray matter structure can be specified employing Maximum Probability Segmentation Maps or even using Spatial Probabilistic Anatomical Maps (Mazziotta et al., 1995). In the future, more advanced graph models should be able to employ both this probability and the uncertainty in the estimation of the fiber orientation distribution function. This, in turn, could be used to estimate the error associated to arc weights, node–node and zone–zone connectivity measures. Additionally, future studies in animals should be addressed to further testing of the performance of the proposed methodology.

Acknowledgments

Authors would like to thank Nelson Rubal Lorenzo, Agustín Lage-Castellanos and Erick C. Jones for their useful comments on the anatomical, statistical and algorithmic aspects of this work, respectively. Also, we thank to Roberto C. Sotero and Thomas Koenig, for the final revision of the manuscript.

Appendix A. Algorithm to solve the most probable path problem

Given a Brain Graph $G_{\text{brain}}=[N,A]$, let us define some quantities before setting up the algorithm:

$|N|$: Cardinality of the set N, i.e. the number of elements belonging to set N.

N^{-s}: Set of nodes that belong to G_{brain} except node 's', $N^{-s}=N/\{\vec{r}_s\}$.

$M(\vec{r}_v)$: Map of probabilities of the path between node 's' and all nodes $\vec{r}_v \in N^{-s}, M(\vec{r}_v)=P[\rho(\vec{r}_s,\vec{r}_v)]$ and $M(\vec{r}_s)=1$.

N_i^{neig}: Nearest neighborhood of the i-th node.

This algorithm proceeds in $|N|-1$ iterations as follows:

a) Set initially:

a.1) $\tilde{S}=N^{-s}$

a.2) $$M(\vec{r}_i)=\begin{cases}1, & \vec{r}_i=\vec{r}_s,\\ w(a_{si}), & \vec{r}_i\in N_i^{\text{neig}}\\ 0, & \text{otherwise.}\end{cases}$$

a.3) $\tilde{\rho}(\vec{r}_s,\vec{r}_i)=a_{si}, \quad \forall \vec{r}_i \in N_s^{\text{neig}}$

b) Find $\vec{r}_j \in \tilde{S}$ such that $M(\vec{r}_j)=\max_{\forall \vec{r}_i \in \tilde{S}} M(\vec{r}_i)$

b.1) Set a new $\tilde{S} \leftarrow \tilde{S}/\{\vec{r}_j\}$

b.2) If $\tilde{S}=\emptyset$, then **Stop**; else continue

c) For all $\vec{r}_m \in N_j^{\text{neig}}$ and $\vec{r}_m \in \tilde{S}$, set

c.1) $\rho(\vec{r}_s,\vec{r}_m)=\{\tilde{\rho}(\vec{r}_s,\vec{r}_j)\cup a_{jm}\}$,

c.2) If $P[\rho(\vec{r}_s,\vec{r}_m)]>M(\vec{r}_m)$ then

$$\tilde{\rho}(\vec{r}_s,\vec{r}_m)=\rho(\vec{r}_s,\vec{r}_m),\ M(\vec{r}_m)=P[\tilde{\rho}(\vec{r}_s,\vec{r}_m)]$$

c.3) **go to b**.

Finally, the map $M(\vec{r}_p)$ for $\vec{r}_p \in N^{-s}$ represents the final probability of the path of maximum reliability according to Eq. (8) between nodes $\vec{r}_s$ and $\vec{r}_p$ denoted by $\tilde{\rho}(\vec{r}_s, \vec{r}_p)$.

Appendix B. White matter orientational distribution function

The intravoxel white matter orientational distribution function (ODF) $\Psi(\hat{u})$ is defined as the radial projection of the probability density function (PDF) $P(\vec{R})$ (Wedeen et al., 2005):

$$\psi(\hat{u}) = \int_0^{+\infty} R^2 P(\hat{u}R)\mathrm{d}R, \tag{B1}$$

being $\hat{u}$ a unitary vector and $\vec{R} = \hat{u}R$ the relative spin displacement.

Considering the PDF for anisotropic Gaussian diffusion:

$$P\left(\vec{R}\right) = (4\pi t)^{-3/2}(|D|)^{-1/2} e^{\frac{-\vec{R}^T D^{-1}\vec{R}}{4t}}, \tag{B2}$$

Then, substituting in Eq. (B1) and using the identity:

$$\int_0^{+\infty} x^m e^{ax^2} dx = \frac{\Gamma\left(\frac{(m+1)}{2}\right)}{2a^{\frac{m+1}{2}}}, \tag{B3}$$

where Γ is the Gamma function, we can obtain the ODF as:

$$\psi(\hat{u}) = \frac{1}{C}\left(\hat{u}^T D^{-1}\hat{u}\right)^{-\frac{3}{2}} \tag{B4}$$

Here, C is a normalization constant which ensures that the ODF is properly normalized to unit mass.

References

Alemán-Gómez, Y., Melie-García, L., Valdes-Hernández, P., 2006. IBASPM: Toolbox for automatic parcellation of brain structures. Presented at the 12th Annual Meeting of the Organization for Hum. Brain Mapp., June 11–15, 2006, Florence, Italy. Available on CD-Rom in NeuroImage, Vol. 27, No.1.

Alexander, D.C., 2005. Multiple-fiber reconstruction algorithms for diffusion MRI. Ann. N. Y. Acad. Sci. 1064, 113–133.

Alexander, D.C., Pierpaoli, C., Basser, P.J., Gee, J.C., 2001. Spatial transformations of diffusion tensor magnetic resonance images. IEEE Trans. Med. Imag. 20, 1131–1139.

Ashburner, J., Friston, K.J., 1999. Nonlinear spatial normalization using basis functions. Hum. Brain Mapp. 7, 254–266.

Ashburner, J., Friston, K.J., 2000. Voxel-based morphometry-the methods. NeuroImage 11, 805–821.

Basser, P.J., Pajevic, S., 2000. Statistical artifacts in diffusion tensor MRI (DT-MRI) caused by background noise. Magn. Reson. Med. 44, 41–50.

Basser, P.J., Mattiello, J., LeBihan, D., 1994. Estimation of the effective self-diffusion tensor from the NMR spin echo. J. Magn. Reson., Ser. B. 103, 247–254.

Basser, P.J., Pajevic, S., Pierpaoli, C., Duda, J., Aldroubi, A., 2000. In vivo fiber tractography using DT-MRI data. Magn. Reson. Med. 44, 625–632.

Behrens, T.E., Johansen-Berg, H., Woolrich, M.W., Smith, S.M., Wheeler-Kingshott, C.A., Boulby, P.A., Barker, G.J., Sillery, E.L., Sheehan, K., Ciccarelli, O., Thompson, A.J., Brady, J.M., Matthews, P.M., 2003. Non-invasive mapping of connections between human thalamus and cortex using diffusion imaging. Nat. Neurosci. 6, 750–757.

Collins, D.L., Neelin, P., Peters, T.M., Evans, A.C., 1994. Automatic 3D intersubject registration of MR volumetric data in standardized Talairach space. J. Comput. Assist. Tomogr. 18, 192–205.

Conturo, T.E., Lori, N.F., Cull, T.S., Akbudak, E., Snyder, A.Z., Shimony, J.S., McKinstry, R.C., Burton, H., Raichle, M.E., 1999. Tracking neuronal fiber pathways in the living human brain. Proc. Natl. Acad. Sci. U. S. A. 96, 10422–10427.

Dijkstra, E.W., 1959. A note on two problems in connexion with graphs. Numer. Math. 269–271.

Efron, B., 2004. Large-scale simultaneous hypothesis testing: the choice of a null hypothesis. J. Am. Stat. Assoc. 99, 96–104.

Efron, B., 2005. Local false discovery rates. http://www-stat.stanford.edu/~brad/papers/.

Evans, A.C., Collins, D.L., 1993. A 305-member MRI-based stereotactic atlas for CBF activation studies. Proceedings of the 40th Annual Meeting of the Society for Nuclear Medicine.

Evans, A.C., Collins, D.L., Neelin, P., MacDonald, D., Kamber, M., Marrett, T.S., 1994. Three-dimensional correlative imaging: applications in human brain mapping. In: Thatcher, R.W., Hallett, M., Zeffiro, T., John, E.R., Huerta, M. (Eds.), Functional Neuroimaging. Technical Foundations, pp. 145–162.

Gómez-Padrón, I., Silva Loynaz, C., Seuc Chiu, A., 1985. Anatomía II. Folleto complementario. Ministerio de salud pública, Cuba.

Gondran, M., Minoux, M., 1984. Graphs and Algorithms. John Wiley and Sons Ltd., Chichester.

Hagmann, P., Thiran, J.P., Jonasson, L., Vandergheynst, P., Clarke, S., Maeder, P., Meuli, R., 2003. DTI mapping of human brain connectivity: statistical fibre tracking and virtual dissection. NeuroImage 19, 545–554.

Hagmann, P., Kurant, M., Gigandet, X., Thiran, P., Wedeen, V.J., Meuli, R., Thiran, J.P., 2006. Imaging the brain neuronal network with diffusion MRI: a way to understand its global architecture. Proc. ISMRM 436.

Hutton, C., Bork, A., Josephs, O., Deichmann, R., Ashburner, J., Turner, R., 2002. Image distortion correction in fMRI: a quantitative evaluation. NeuroImage 16, 217–240.

Iturria-Medina, Y., Valdes-Hernandez, P., Canales-Rodriguez, E., 2005. Measures of anatomical connectivity obtained from neuro diffusion images. Available on CD-Rom in NeuroImage, Vol. 26, No.1; Presented at the 11th Annual Meeting of the Organization for Hum. Brain Mapp., June 12–16, 2005, Toronto, Ontario, Canada.

Jansons, K.M., Alexander, D.C., 2003. Persistent angular structure: new insights from diffusion MRI data. Dummy version. Inf. Process. Med. Imag. 18, 672–683.

Jones, D.K., Horsfield, M.A., Simmons, A., 1999. Optimal strategies for measuring diffusion in anisotropic systems by magnetic resonance imaging. Magn. Reson. Med. 42, 515–525.

Jun Zhang, Hao Ji, Ning Kang and Ning Cao, 2005. Fiber Tractography in Diffusion Tensor Magnetic Resonance Imaging: A Survey and Beyond. Technical Report No. 437-05 ed., Department of Computer Science; University of Kentucky; Lexington; KY.

Koch, M.A., Norris, D.G., Hund-Georgiadis, M., 2002. An investigation of functional and anatomical connectivity using magnetic resonance imaging. NeuroImage 16, 241–250.

Lazar, M., Weinstein, D.M., Tsuruda, J.S., Hasan, K.M., Arfanakis, K., Meyerand, M.E., Badie, B., Rowley, H.A., Haughton, V., Field, A., Alexander, A.L., 2003. White matter tractography using diffusion tensor deflection. Hum. Brain Mapp. 18, 306–321.

LeBihan, D., 2003. Looking into the functional architecture of the brain with diffusion MRI. Nat. Rev., Neurosci. 4, 469–480.

LeBihan, D., Mangin, J.F., Poupon, C., Clark, C.A., Pappata, S., Molko, N., Chabriat, H., 2001. Diffusion tensor imaging: concepts and applications. J. Magn. Reson. Imaging 13, 534–546.

Lori, N.F., Akbudak, E., Shimony, J.S., Cull, T.S., Snyder, A.Z., Guillory, R.K., Conturo, T.E., 2002. Diffusion tensor fiber tracking of human brain connectivity: acquisition methods, reliability analysis and biological results. NMR Biomed. 15, 494–515.

Mazziotta, J.C., Toga, A.W., Evans, A., Fox, P., Lancaster, J., 1995. A probabilistic atlas of the human brain: theory and rationale for its development. The International Consortium for Brain Mapping (ICBM). NeuroImage 2, 89–101.

Moore, E.F., 1959. The Shortest Path Through a Maze. Harvard University Press, Cambridge, Massachusetts, pp. 285–292.

Mori, S., van Zijl, P.C., 2002. Fiber tracking: principles and strategies—A technical review. NMR Biomed. 15, 468–480.

Mori, S., Crain, B.J., Chacko, V.P., van Zijl, P.C., 1999. Three-dimensional tracking of axonal projections in the brain by magnetic resonance imaging. Ann. Neurol. 45, 265–269.

Parker, G.J., Alexander, D.C., 2003. Probabilistic Monte Carlo based mapping of cerebral connections utilising whole-brain crossing fibre information. Inf. Process. Med. Imag. 18, 684–695.

Parker, G.J., Wheeler-Kingshott, C.A., Barker, G.J., 2002. Estimating distributed anatomical connectivity using fast marching methods and diffusion tensor imaging. IEEE Trans. Med. Imag. 21, 505–512.

Parker, G.J., Haroon, H.A., Wheeler-Kingshott, C.A., 2003. A framework for a streamline-based probabilistic index of connectivity (PICo) using a structural interpretation of MRI diffusion measurements. J. Magn. Reson. Imaging 18, 242–254.

Ramnani, N., Behrens, T.E., Penny, W., Matthews, P.M., 2004. New approaches for exploring anatomical and functional connectivity in the human brain. Biol. Psychiatry 56, 613–619.

Sotero, R.C., Trujillo-Barreto, N.J., Iturria-Medina, Y., Carbonell, F., Jimenez, J.C., 2007. Realistically coupled neural mass models can generate EEG rhythms. Neural Comput. 19, 478–512.

Sporns, O., Tononi, G., Kotter, R., 2005. The human connectome: a structural description of the human brain. PLoS. Comput. Biol. 1, e42.

Staempfli, P., Jaermann, T., Crelier, G.R., Kollias, S., Valavanis, A., Boesiger, P., 2006. Resolving fiber crossing using advanced fast marching tractography based on diffusion tensor imaging. NeuroImage 30, 110–120.

Standring, S., 2004. Gray's Anatomy: The Anatomical Basis of Medicine and Surgery, 39th edition. Churchill Livingstone.

Studholme, Hill, Hawkes, 1998. A normalized entropy measure of 3-D medical alignment. Proc. Med. Imaging, vol. 3338. SPIE Press, San Diego, CA, pp. 132–143.

Tench, C.R., Morgan, P.S., Blumhardt, L.D., Constantinescu, C., 2002. Improved white matter fiber tracking using stochastic labeling. Magn. Reson. Med. 48, 677–683.

Tuch, D.S, 2002. MRI of complex tissue structure. PhD Thesis.

Tuch, D.S., 2004. Q-ball imaging. Magn. Reson. Med. 52, 1358–1372.

Wedeen, V.J., Hagmann, P., Tseng, W.Y., Reese, T.G., Weisskoff, R.M., 2005. Mapping complex tissue architecture with diffusion spectrum magnetic resonance imaging. Magn. Reson. Med. 54, 1377–1386.

Weinstein, D., Kindlmann, G., Lundberg, E., 1999. Tensorlines: advection-diffusion based propagation through diffusion tensor fields. Proc. IEEE Visualization, San Francisco, CA, pp. 249–253.

Witelson, S.F., 1989. Hand and sex differences in the isthmus and genu of the human corpus callosum. A postmortem morphological study. Brain 112 (Pt. 3), 799–835.

Yakoub, B., Lorenzo, B., Farid, M., 2006. Image thresholding based on the EM algorithm and the generalized Gaussian distribution. Pattern Recogn. 40, 619–634.

Young, M.P., 1993. The organization of neural systems in the primate cerebral cortex. Proc. Biol. Sci. 252, 13–18.